

Neurological dysfunctions in mice expressing different levels of the Q/R site-unedited AMPAR subunit GluR-B

Dirk Feldmeyer², Kalev Kask^{1,4}, Rossella Brusa^{1,5}, Hans-Christian Kornau^{1,6}, Rohini Kolhekar^{1,6}, Andrei Rozov², Nail Burnashev², Vidar Jensen³, Øivind Hvalby³, Rolf Sprengel¹ and Peter H. Seeburg¹

¹ Department of Molecular Neurobiology and ²Department of Molecular Cell Physiology, Max-Planck-Institute for Medical Research, Jahnstr. 29, 69120 Heidelberg, Germany

³ Institute of Neurophysiology, University of Oslo, P.O. Box 1104 Blindern, N-0317 Oslo, Norway

⁴ Present address: AGY Therapeutics, Inc., c/o Tularik, Inc., Two Corporate Drive, South San Francisco, California 94080, USA

⁵ Present address: Schering Plough Research Institute, Via Olgettina 58, 20132, Milan, Italy

⁶ Present address: BASF-LYNX Bioscience AG, Im Neuenheimer Feld 515, 69120 Heidelberg, Germany

Correspondence should be addressed to R.S. (sprengel@mpimf-heidelberg.mpg.de)

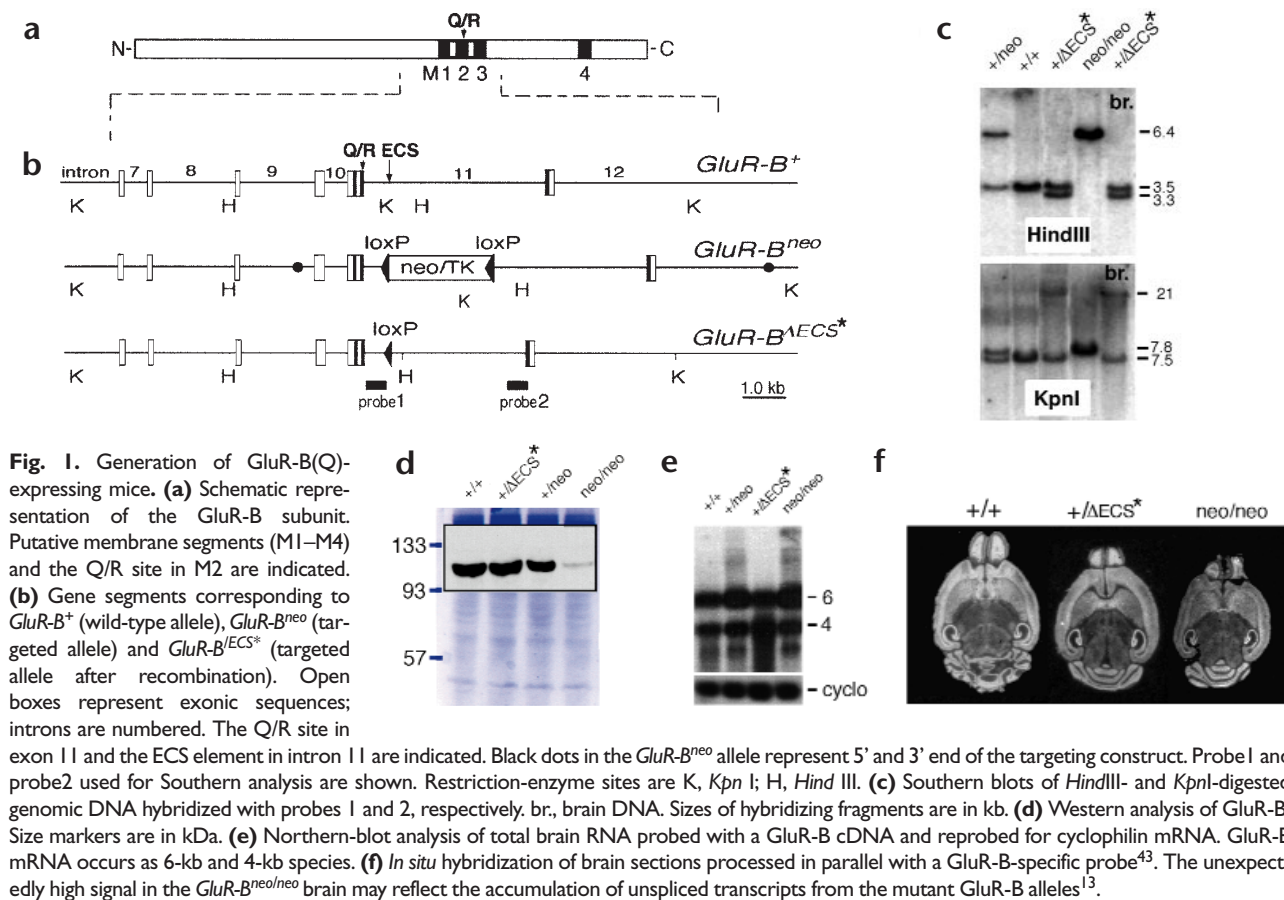
We generated mouse mutants with targeted AMPA receptor (AMPA) GluR-B subunit alleles, functionally expressed at different levels and deficient in Q/R-site editing. All mutant lines had increased AMPAR calcium permeabilities in pyramidal neurons, and one showed elevated macroscopic conductances of these channels. The AMPAR-mediated calcium influx induced NMDA-receptor-independent long-term potentiation (LTP) in hippocampal pyramidal cell connections. Calcium-triggered neuronal death was not observed, but mutants had mild to severe neurological dysfunctions, including epilepsy and deficits in dendritic architecture. The seizure-prone phenotype correlated with an increase in the macroscopic conductance, as independently revealed by the effect of a transgene for a Q/R-site-altered GluR-B subunit. Thus, changes in GluR-B gene expression and Q/R site editing can affect critical architectural and functional aspects of excitatory principal neurons.

Establishment, maintenance and elimination of synaptic connections during central nervous system (CNS) development are controlled by calcium influx through glutamate receptor (GluR) channels¹. Synaptic calcium influx through these channels is also required to induce long-term changes in the efficacy of synaptic connections². Excessive calcium influx, on the other hand, is toxic and causes neuronal degeneration and sclerosis^{3,4}.

The AMPAR subtype of GluR channels, composed predominantly of heteromeric subunit assemblies (reviewed in ref. 5), mediates fast excitatory transmission. Its calcium permeability is minimal in principal glutamatergic neurons, but is increased over a 20-fold range in other neuronal classes^{6,7}. The low calcium permeability of AMPARs in pyramidal neurons results from higher expression of the GluR-B subunit than of other AMPAR subunits⁶. The GluR-B subunit imparts low calcium permeability to AMPARs because it carries an arginine (R) residue in its pore-forming M2 segment^{8,9}, in a position occupied by glutamine (Q) in the other AMPAR subunits⁵. The critical arginine residue at this 'Q/R site' is not exonically encoded; rather, its codon (CIG) is created at the pre-mRNA stage by site-selective adenosine deamination within the Q/R site codon CAG¹⁰ (reviewed in ref. 11). Thus, heterozygous carriers of a modified GluR-B allele (*GluR-B^{ΔECS}*), which are rendered editing deficient by replacement of the intronic cis-acting editing site complementary sequence (ECS)¹² with a loxP sequence, show increased AMPAR calcium permeability, which manifests in epileptic seizures and premature death¹³. By contrast, GluR-B-deficient

mice are mostly viable, with impairments in open-field behavior and motor coordination¹⁴, even though the absence of GluR-B increases the calcium permeability of AMPARs to its maximum. Besides differences in genetic background, the conflicting phenotypic consequences may reflect differences in the number, localization and ability to interact with cellular proteins of AMPARs with or without GluR-B, because the presence of GluR-B may enhance AMPAR assembly¹⁵ and may mediate proximity to particular subsynaptic signaling components^{16–18}. In addition, the magnitude of calcium inflow is determined not only by the calcium permeability of AMPAR channels, but also by channel number, single-channel conductance^{19,20}, gating kinetics^{21,22} and current rectification^{23,24}, parameters that are all affected by GluR-B levels and by edited versus unedited GluR-B subunits.

We have now investigated the consequences of different expression levels of calcium-permeable and -impermeable GluR-B forms in mice. To generate the mutants, we built on our observation that ECS substitution in intron 11 by loxP slowed splicing of that intron¹³, producing a twofold drop in mRNA levels relative to the wild-type allele. We enhanced the 'silencing' effect for the editing-deficient allele by leaving in the intron the loxP-flanked marker genes. Furthermore, a GluR-B transgene (*GluR-B^{Ntrans}*) with increased calcium influx was introduced into the mouse genome. By combining the different GluR-B alleles, we were able to compare mouse mutants whose principal neurons differed in the magnitude of AMPAR-mediated calcium influx and in macroscopic AMPAR conductances.



Results

GLUR-B(Q) EXPRESSION OF MODIFIED GLUR-B ALLELES

C57BL/6 blastocysts were injected with recombinant mouse embryonic stem (ES) cells¹³, targeted for substitution of the ECS element in the *GluR-B* gene by a cassette composed of the neomycin resistance (*neo*) and thymidine kinase (*tk*) genes and flanked by *loxP* sites (Fig. 1a and b). Two chimeras transmitted the modified GluR-B allele (*GluR-B*^{neo}) through the germline, and heterozygous carriers were used to generate mice differing in *GluR-B* genotype.

First, *GluR-B*^{+/neo} intercrosses gave rise to *GluR-B*^{neo/neo} mice. Second, when crossed with the *Cre-deleter*²⁵, the 'floxed' *neo-tk* cassette was removed, as judged by Southern-blot analysis of liver and brain DNA from offspring that carried both the *GluR-B*^{neo} allele and the *Cre* transgene (Fig. 1c). The allele generated by *in-vivo* excision of the *neo-tk* cassette is designated *GluR-B*^{ΔECS*} to distinguish it from the *GluR-B*^{ΔECS} allele that resulted from transient *Cre* expression in targeted ES cells¹³. As expected from the *GluR-B*^{ΔECS} mice, GluR-B subunit levels in the forebrain depended on the GluR-B genotype, with high GluR-B levels in wild-type and *GluR-B*^{+/ΔECS*} mice, intermediate levels in *GluR-B*^{+/neo} mice and low levels in *GluR-B*^{neo/neo} mice (Fig. 1d).

Changed GluR-B expression was not obvious when we analyzed total brain RNA by northern blot and *in situ* hybridization (Fig. 1e and f). However, a transcript analysis with allele-specific oligonucleotides to probe cloned GluR-B RT-PCR products¹² revealed that *GluR-B*^{neo} mRNA constituted only about 10% of the entire GluR-B mRNA in *GluR-B*^{+/neo} mice. The reduced mRNA of the *GluR-B*^{neo} allele might reflect premature transcriptional ter-

mination and splicing alterations within the *neo-tk* cassette²⁶ or nuclear accumulation of unspliced transcripts, as described for the *GluR-B*^{+/ΔECS} allele, which contributed approximately 30% of the entire GluR-B mRNA¹³.

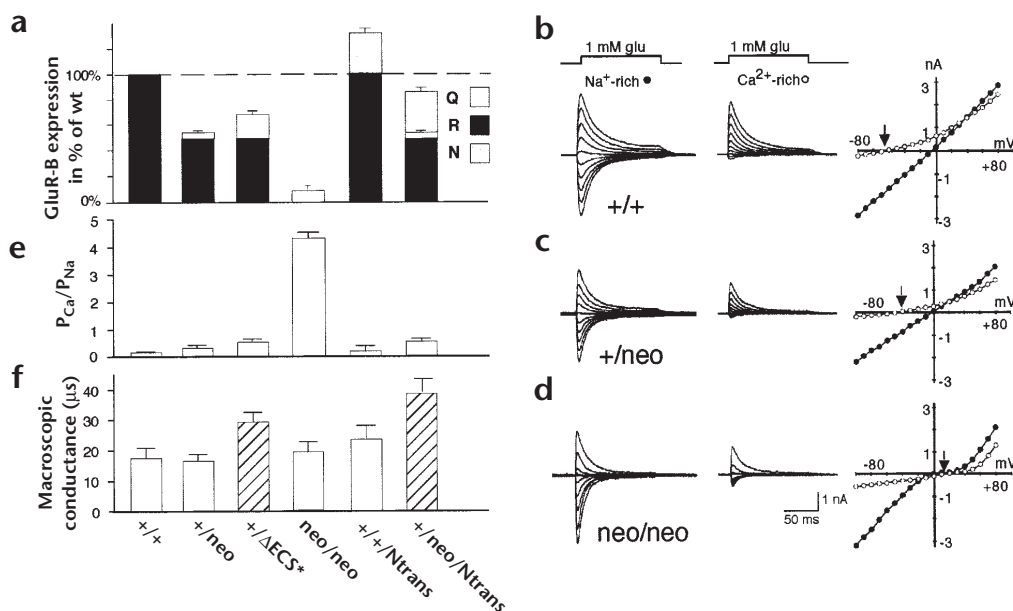
Thus, using allelic mRNA levels as expression indicators, GluR-B subunit levels were found to be 60%, 80% and 10% of wild type in *GluR-B*^{+/neo}, *GluR-B*^{+/ΔECS*} and *GluR-B*^{neo/neo} mice, respectively (Fig. 2a). Moreover, because *GluR-B*^{neo} and *GluR-B*^{ΔECS*} transcripts cannot be edited at the Q/R site, the GluR-B(R) subunit percentage that remains wild type is 0% in the *neo/neo* and 50% in the *+/ΔECS** and *+/neo* genotypes (Fig. 2a). Despite these changes, the expression of GluR-A, -C and -D and NMDAR1 mRNAs remained unchanged, as determined by *in situ* hybridization (not shown).

CALCIUM INFLOW AND CONDUCTANCE OF AMPARs

Analysis of AMPARs of pyramidal neurons in the hippocampal CA1 subfield revealed differences in current rectification and relative calcium permeability (P_{Ca}/P_{Na}) dependent on the genotype (Fig. 2b–e). The effects were pronounced in *GluR-B*^{neo/neo} mice, which express GluR-B only as the Q-form. The reversal potential of AMPAR-mediated currents was shifted from 0.3 ± 0.8 mV (mean \pm standard error) to 12.4 ± 0.9 mV ($n = 7$) by switching from sodium-rich to calcium-rich solution (Fig. 2d), as expected for AMPARs assembled solely from subunits in their Q-form²⁷. Reflecting the voltage-dependent block by spermine in such AMPARs^{23,24}, the currents rectified strongly. Furthermore, AMPAR currents in *GluR-B*^{neo/neo} mice desensitized faster and had a smaller steady-state component than in wild-type mice and the other mutants (Fig. 2d). As GluR-B, at

Fig. 2. Calcium permeability and macroscopic conductance of AMPARs in pyramidal neurons.

(a) Graphic representation of allelic GluR-B mRNA levels. The expression of both wild-type GluR-B alleles is defined as 100%. Black bars represent the levels of GluR-B(R), white bars GluR-B(Q) and gray bars GluR-B(N) (see Fig. 5). **(b–d)** AMPAR-mediated currents were elicited by 1 mM glutamate in nucleated patches from CA1 pyramidal neurons at different membrane potentials in sodium-rich (left) and calcium-rich (right) extracellular solution. Also shown are corresponding I–V relations of AMPAR-mediated currents in physiological (filled circles) and high calcium (open circles) ionic conditions. Arrows, reversal potential in high extracellular calcium solution. **(e)** Relative calcium permeability (P_{Ca}/P_{Na}) of AMPAR channels in hippocampal CA1 pyramidal cells. **(f)** Macroscopic AMPAR-mediated conductances as measured in nucleated patches of CA1 pyramidal neurons. The conductance is highest (hatched bars) in the two mutants with seizure-prone phenotype. Genotypes indicated on the x-axis of (f) also apply to panels (a) and (e).



least in its R form, confers slow gating kinetics but fast recovery from desensitization^{9,21,22}, properties that increase the steady-state component, this result suggests that most AMPARs in pyramidal cells of *GluR-B^{neo/neo}* mice do not contain GluR-B, consistent with the low amount of GluR-B(Q) in this line. The AMPARs in *GluR-B^{+ΔECS*}* animals had properties like those described, with a fivefold increased calcium permeability in CA1 pyramidal cells (Table 1) and a small degree of current rectification¹³. However, in *GluR-B^{+neo}* mice, calcium permeability was increased only approximately twofold (Table 1), and the lack of current rectification was comparable to wild-type responses (Fig. 2b and c).

The fractional calcium currents (P_f) through AMPAR channels were calculated from constant-field assumptions²⁷. At a membrane potential of -60 mV, the increase relative to wild type in P_f values of AMPARs in CA1 pyramidal cells was 2-fold in *GluR-B^{+neo}*, 4.5-fold in *GluR-B^{+ΔECS*}* and 29-fold in *GluR-B^{neo/neo}* mice (Table 1). To reveal changes in macroscopic AMPAR-mediated conductances due to altered channel number and/or single-channel conductance, we compared AMPAR currents in nucleated patches as calculated by

the averaged peak amplitudes corrected for reversal potential at -70 mV. All AMPAR conductances were similar except those of *GluR-B^{+ΔECS*}* mice, which were significantly increased (Table 1).

LONG-TERM POTENTIATION IN HIPPOCAMPAL CONNECTIONS

Long-term changes in synaptic function were studied in the hippocampal CA1 field in brain slices from adult *GluR-B^{+neo}* and young *GluR-B^{+ΔECS*}* and *GluR-B^{neo/neo}* mice. Tetanic stimulation of afferent fibers, in either stratum radiatum or stratum oriens (Fig. 3a), elicited a persistent homosynaptic potentiation of the synaptic responses characteristic of LTP, measured as an increased slope of the field excitatory postsynaptic potentials (fEPSP)²⁸. As with rats²⁹, LTP after 45 minutes was the same size in adult (mean \pm standard error, $148 \pm 9\%$, $n = 18$ in 7 animals) and young ($142 \pm 10\%$, $n = 22$ slices from 8 animals) wild-type mice (Fig. 3b). A similar amount of LTP was obtained in slices from the mutants. A slightly smaller LTP was observed in *GluR-B^{neo/neo}* mice ($136 \pm 10\%$; $n = 9$ slices from 5 animals), but this result was not statistically different ($p > 0.1$) from wild-type values.

Table 1. Expression of GluR-B alleles and changed AMPAR properties.

	GluR-B alleles					
	+/+	+/neo	+/ΔECS*	neo/neo	+/+Ntrans	+/neoNtrans
GluR-B mRNA (% Q)	<0.1	8.7 \pm 2.5	27.8 \pm 4.7	98 \pm 1.2	24 \pm 2 ^a	~45 ^b
GluR-B protein (R+Q) (% wt)	100	~60	~80	~10	~130 ^c	~100 ^c
P_{Ca}/P_{Na} (\pm standard error)	0.13 \pm 0.01	0.28 \pm 0.02	0.58 \pm 0.04	4.34 \pm 0.17	0.17 \pm 0.04	0.59 \pm 0.09
P_f (fold wt)	1	2	4.5	29	1.5	4.5
γ (nS \pm standard error)	18 \pm 3	17 \pm 2	30 \pm 3	20 \pm 3	24 \pm 4	39 \pm 4

Transcript levels ($n \geq 6$) were obtained from differential hybridization analysis¹² of GluR-B RT-PCR fragments. Subunit levels ($n \geq 2$) are from western blots analyzed by NIH Image software package (NIH Image 1.57). P_{Ca}/P_{Na} , relative calcium permeability in CA1 neurons ($n \geq 6$), as calculated from reversal potentials. Fractional calcium currents (P_f) were calculated from corresponding calcium permeabilities for recombinantly expressed AMPARs. γ , macroscopic AMPAR conductance in nucleated CA1 pyramidal cell patches ($n > 6$). ^a % N; ^b % Q+N; ^c R+Q+N (% wt). wt, wild-type.

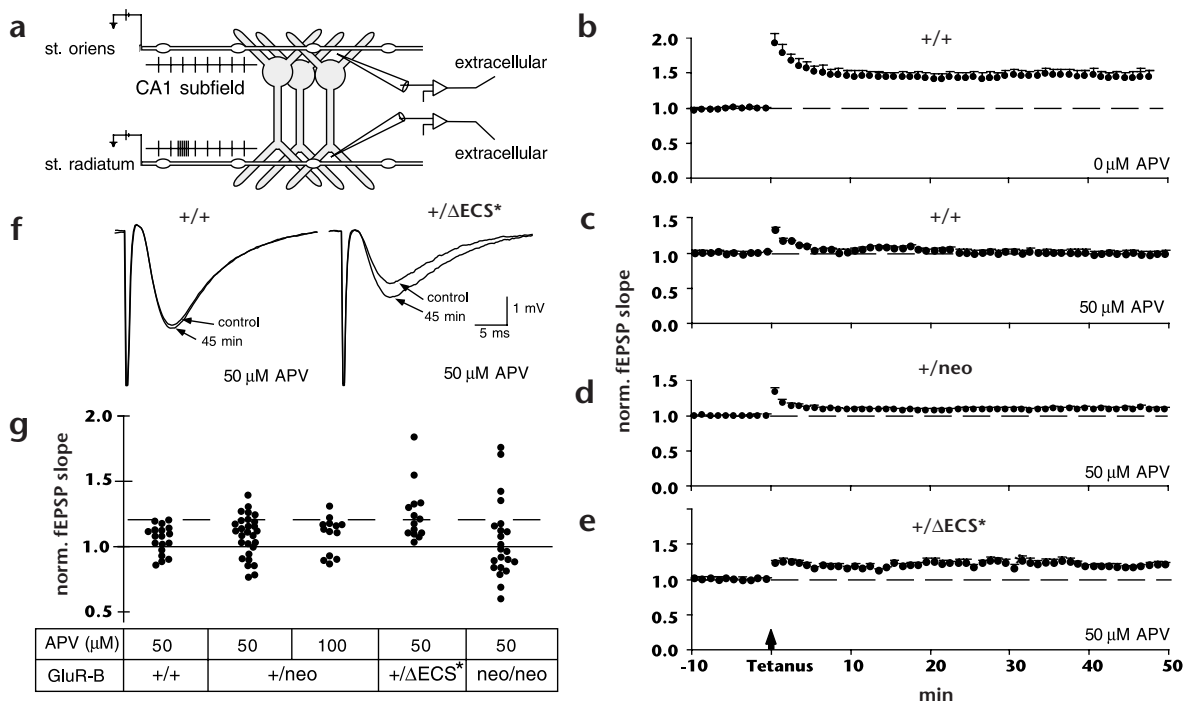


Fig. 3. NMDAR-independent LTP. **(a)** Electrode arrangement. Electrodes in stratum radiatum and stratum oriens were stimulated alternately. Radiatum fibers served as the tetanizing input, oriens fibers as the control or vice versa. The field synaptic responses were monitored by a recording electrode in stratum radiatum. **(b–e)** Averaged fEPSP measurements in control solution (**b**) and in presence of APV (**c–e**). The control pathway is indicated by a broken line; arrow denotes time of tetanus. **(f)** Synaptic responses in wild-type and *GluR-B*^{+/ ΔECS^*} mice in the presence of 50 μM APV before and after desensitization. **(g)** Normalized fEPSP slope of different GluR-B mutants in the presence of 50 μM APV (for +/neo, also 100 μM APV) and 2 mM calcium 45 minutes after tetanus.

As LTP induction in CA1 critically depends on NMDAR activation², we blocked these channels pharmacologically to determine if calcium-permeable AMPARs can substitute for NMDARs during LTP induction^{14,30,31}. As expected, 50 μM APV blocked LTP in wild-type animals (adult, 105 \pm 3% tetanized versus 105 \pm 2% control, $n = 18$ slices from 4 animals; young, 104 \pm 5% versus 104 \pm 3%, $n = 18$ slices from 6 animals) (Fig. 3c, f and g). In the presence of APV, *GluR-B*^{+/*neo*} mice showed only a tendency toward enhancement of the tetanized pathway (50 μM APV, 109 \pm 3% versus 105 \pm 2%, $n = 28$ slices from 6 animals, $p = 0.23$; 100 μM APV, 109 \pm 4% versus 104 \pm 2%, $n = 13$ slices from 4 animals, $p = 0.16$; Fig. 3d). LTP induction critically depends on the extracellular calcium concentration^{32,33}. When calcium was raised to 4 mM, 50 μM APV still blocked LTP in wild-type mice (100 \pm 5% versus 97 \pm 3%, tetanized versus control pathway, $n = 18$ slices from 4 animals). In high calcium, *GluR-B*^{+/*neo*} mice showed a small enhancement (112 \pm 5% versus 97 \pm 3%, $n = 15$ slices from 3 animals; $p = 0.03$, two-tailed), which did not reach our criterion of 120% of control.

GluR-B^{+/ ΔECS^*} mice develop seizures¹³, but hippocampal slice preparations from such animals (P11–17) showed neither hyperexcitability nor epileptiform activity. In 50 μM APV and 2 mM calcium, substantial LTP was measured in the tetanized pathway in slices of *GluR-B*^{+/ ΔECS^*} mice (125 \pm 6% versus 103 \pm 4% in the control pathway, $n = 14$ slices from 3 animals, $p = 0.01$; Fig. 3e, f and g), surpassing our standard criteria for LTP (120% of the pretetanic value 45 min after tetanization).

GluR-B^{neo/neo} mice showed a larger variance of LTP magnitude than *GluR-B*^{+/ ΔECS^*} mice (Fig. 3g). Notably, several slices (4 of 22)

from *GluR-B*^{neo/neo} mice had substantial LTP development in APV, with values as high (LTP index >1.5; Fig. 3g) as in *GluR-B*^{+/ ΔECS^*} mice. We observed that *GluR-B*^{neo/neo} mice required 30% higher stimulation currents to elicit fEPSPs of the same amplitude as wild-type mice, possibly reflecting deficits in neuronal morphology.

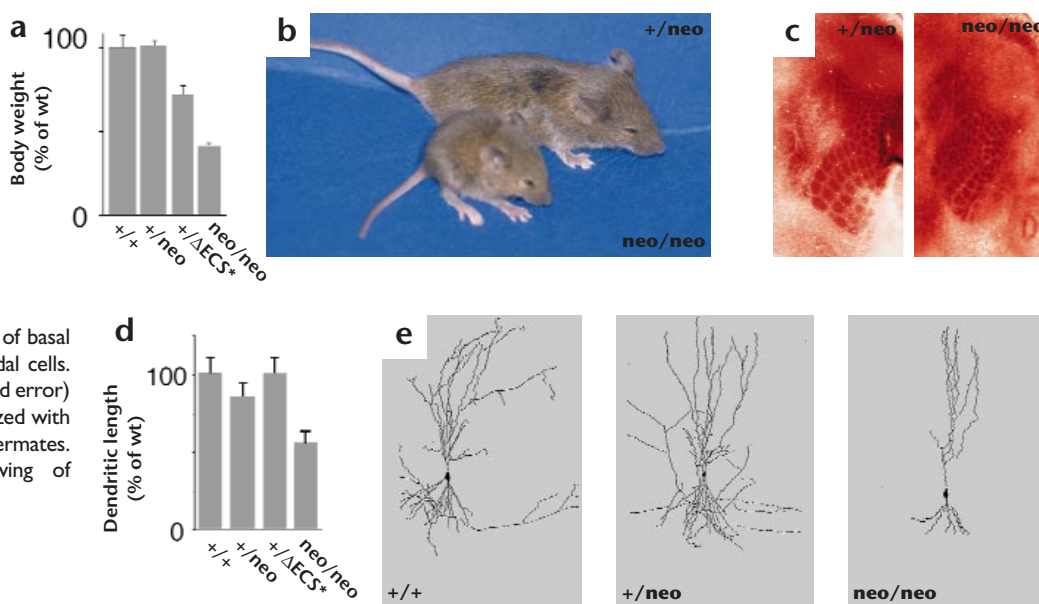
NEUROLOGICAL PHENOTYPES AND BRAIN ANATOMY

The mutant alleles generated different phenotypes (Table 2). The *GluR-B*^{+/*neo*} mice were least affected. The *GluR-B*^{+/ ΔECS^*} mutant developed a seizure-prone phenotype and premature lethality. *GluR-B*^{neo/neo} mice showed strong developmental deficits, were severely hypomorphic (Fig. 4a and b), showed stupor from P15 onward and did not survive to P20. These animals were hypoexcitable, in part probably because of cytoarchitectural deficits. The premature lethality of *GluR-B*^{+/ ΔECS^*} and *GluR-B*^{neo/neo} mice could have resulted from abnormal or insufficient neuronal connections made in the developing CNS, or it could reflect acute neurodegenerative changes. However, Nissl-stained sections of hippocampus and cortex of P15–20 animals appeared normal in cell density and number. Neurosclerosis was observed by hematoxylin-eosin staining in the lateral CA3 subfield upon postmortem analysis of *GluR-B*^{+/ ΔECS^*} mice that had undergone prolonged seizure episodes.

To reveal possible deficits in CNS architecture, we examined individual hippocampal CA3 and CA1 neurons by biocytin labeling³⁴ at P16. Analysis of camera-lucida reconstructions of pyramidal neurons ($n = 5$) showed that in *GluR-B*^{neo/neo} animals the basal dendrites of CA3 cells are reduced in length (total \pm standard deviation, 1535.6 \pm 590.7 μm versus 3708.7 \pm 1595 μm in wild-type; mean \pm standard deviation, 456.6 \pm 162.1 μm versus 934.2 \pm 720.7

Fig. 4. Phenotypes and structural deficits in neuronal architecture.

(a) Averaged body weight of mutants at P17. **(b)** Comparative photograph of two mutants. **(c)** Barrel-field architecture in somatosensory neocortex as shown by cytochrome oxidase staining. **(d)** Arborization of basal dendrites of CA3 pyramidal cells. The data (means \pm standard error) in each group are normalized with respect to wild-type littermates. **(e)** Camera-lucida drawing of CA3 pyramidal cells.



μm in wild-type) and in number of branching points (11.4 ± 5 versus 29.7 ± 13.2 in wild-type; Fig. 4d and e).

This developmental deficit prompted us to examine barrel-field formation in the primary somatosensory cortex at P12–16 (Fig. 4c). In all mutants, barrel-field structure did not differ from that of wild-type mice. Although we did not examine a possible abnormality in dendritic arborization of neocortical neurons, our results suggest that the increased calcium influx through AMPARs and the deficits in dendritic differentiation do not perturb the activity-dependent structuring of synaptic connections in the neocortex.

GLUR-B(N) TRANSGENIC MICE

To further correlate neurological dysfunction with calcium-permeable GluR-B levels, we generated a transgenic line *GluR-B^{+/+/Ntrans}* (Fig. 5a). In addition to both endogenous GluR-B alleles, these mice carry multiple copies of a GluR-B(N) minigene, which encodes an asparagine (N) at the Q/R site. AMPAR channels incorporating GluR-B(N) are permeable to divalent cations but lack current rectification⁹. A transgenic line was selected in which the GluR-B(N) minigene had an expression pattern similar to that of the endogenous GluR-B, as judged by *in situ* hybridization (Fig. 5b). The transgene of this line expressed GluR-B(N) mRNA to 63% of one wild-type GluR-B allele level (Table 1). Thus, GluR-B expression exceeds wild-type levels (Figs 5c and 2a), and measurements in nucleated CA1 cell patches indicate a twofold increase in the calcium permeability of AMPARs in transgene carriers (Figs 5d and 2e and Table 1). These mice show no overt phenotype until later in life, when they develop a motoneuron disease (Kolkehar *et al.*, *Soc. Neurosci. Abstr.* 24, 599.10, 1998).

When this transgene was introduced into the *GluR-B^{+neo}* line, the combined effect of the *GluR-B^{+neo}* allele and the GluR-B(N) transgene generated a seizure-prone, lethal phenotype (Table 2). In these double heterozygous *GluR-B^{+neo/Ntrans}* mice, the calcium permeability of AMPARs in CA1 pyramidal neurons increased approximately fourfold relative to wild-type (Figs 5d and 2e) and became comparable to that in *GluR-B^{+ΔECS*}* mice (Table 1). The macroscopic

AMPA conductance in nucleated patches of CA1 pyramidal cells was the highest of all mutant lines (Fig. 2f). Postmortem analysis showed neurosclerosis in CA3, similar to that observed in *GluR-B^{+ΔECS*}* mice and probably caused by prolonged seizure episodes. A comparison of AMPAR properties and mouse phenotypes (Tables 1 and 2; Fig. 2e and f) indicates that the seizure-prone phenotype correlates with the macroscopic conductance of GluR-B-containing AMPAR channels. The contributions of the increased AMPAR-mediated sodium and calcium conductances to this phenotype need investigating.

Discussion

Our mutant mouse strains differ from wild-type mice in GluR-B levels and in the extent of Q/R site editing of this subunit. The functional property changes of AMPARs in pyramidal neurons of these mutants generated phenotypes ranging from mild to epileptic lethal and to a lethal hypomorph with deficits in neuronal architecture.

EFFECTS OF GLUR-B EXPRESSION

In animals with a mild phenotype (*GluR-B^{+neo}*), 50% of the GluR-B(R) subunits are replaced by one-tenth as much GluR-B(Q). This reduction in GluR-B(R) expression can be monitored by increased calcium influx through AMPAR channels in CA1 neurons. The GluR-B(R) subunits levels seem to be too low to guarantee that at least one GluR-B(R) subunit is incorporated in every AMPAR channel, so that in the mutants a measurable proportion of the AMPAR becomes permeable to calcium. This view is supported

Table 2. GluR-B mutants and their phenotypes.

GluR-B alleles	phenotype
+/ <i>neo</i>	impaired open-field behavior ^a , slightly increased lethality (20%)
+/ Δ ECS*	hyperexcitable, epileptic, hypomorphic, early death (< P21)
<i>neo/neo</i>	lethargic, severely hypomorphic, dendritic deficits, early death (< P20)
+/ <i>Ntrans</i>	nearly normal, late motoneuron degeneration
+/ <i>neo/Ntrans</i>	hyperexcitable, epileptic, hypomorphic, early death (< P25)

^adefined as in ref. 14.

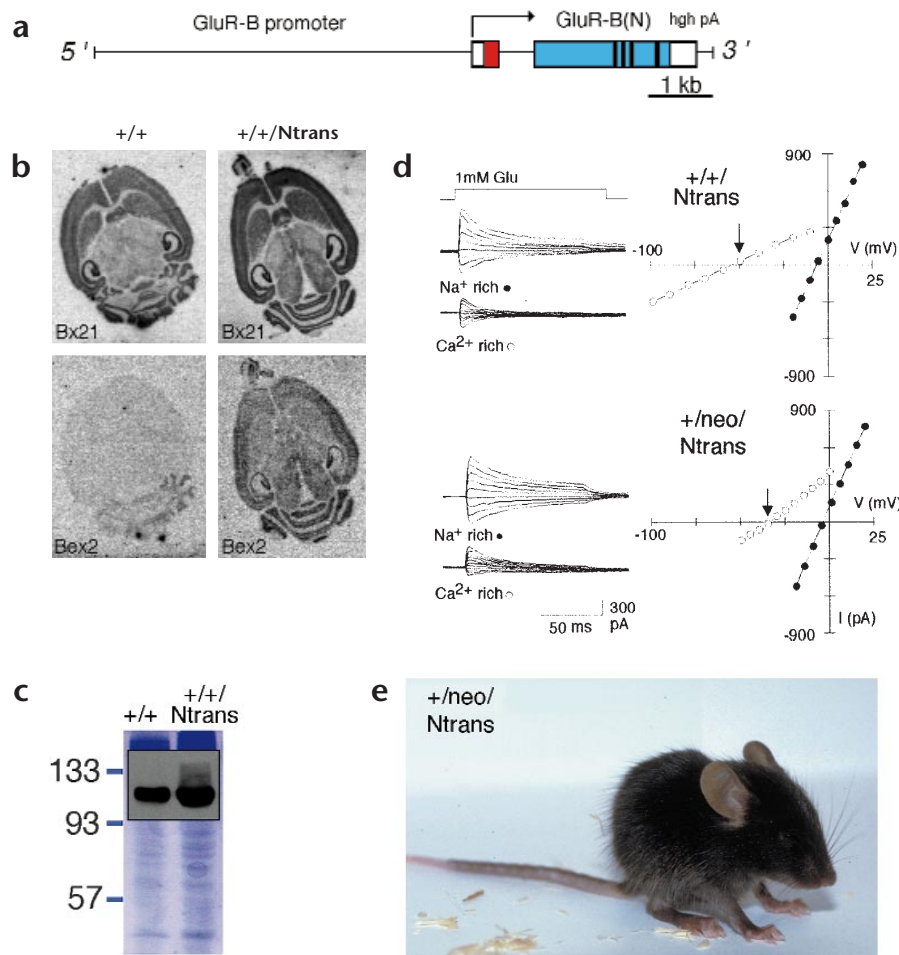


Fig. 5. Expression and effect of a GluR-B(N) transgene. **(a)** Schematic representation of the GluR-B(N) transgene: transcriptional start site (arrow), 5' untranslated sequence (white box), coding sequence (red box, murine; blue box, rat). Membrane insertion domains M1 to M4 are in black, and the Q/R site codon in M2 encodes asparagine (N). **(b)** *In situ* hybridization for total GluR-B mRNA (Bx21 as probe) and for GluR-B(N) mRNA (Bex2 as probe). **(c)** Western blot for GluR-B; size markers are in kDa. **(d)** Current-voltage relationships and reversal potentials in high-sodium and high-calcium solution (arrow) of CA1 pyramidal cells. **(e)** A double heterozygous mouse at P17.

by mice expressing GluR-B(R) at 70% of wild-type levels³⁵ and by *GluR-B^{+/+/Ntrans}* mice, in which the pool of subunits for calcium-permeable AMPAR channels is enlarged by additional GluR-B(N) subunits. AMPARs of both mutants show a similar increase in calcium permeability.

As predicted from the *GluR-B^{+/neo}* and *GluR-B^{+/+/Ntrans}* mutants, calcium-permeable AMPARs should further increase in number with additional levels of GluR-B(Q) or GluR-B(N) subunits. Indeed, in *GluR-B^{+/ΔECS*}* and *GluR-B^{+/neo/Ntrans}* mice, in which 50% of the GluR-B(R) subunits are replaced by about 30% GluR-B(Q) or 5% GluR-B(Q) plus 30% GluR-B(N), the calcium permeability is further increased. However, the macroscopic AMPAR conductance is also enhanced, which may result from both an increase in the number of AMPARs and from the two- to threefold increased single-channel conductance of calcium-permeable AMPARs relative to calcium-impermeable AMPARs^{19,20}. Together with this increase in AMPAR-mediated conductance, we observed in both *GluR-B^{+/ΔECS*}* and *GluR-B^{+/neo/Ntrans}* periodic spontaneous epileptic seizures that start at P14/15 and end with the death of the animals around P20 to P25.

The most severe phenotype was observed for *GluR-B^{neo/neo}*. These mice are retarded in growth and die between P4 and P20; epileptic seizures or periods of hyperactivity were never observed in these mice. Their AMPARs show 30-fold increased calcium permeability, as expected from lack of GluR-B(R). In spite of a threefold increased single-channel conductance of AMPARs^{19,20}, macroscopic

AMPA conductances in hippocampal CA1 pyramidal neurons were comparable to those in wild-type animals, arguing for at least a threefold reduced number of AMPARs in these mutants.

An even stronger reduction in AMPAR-mediated currents in CA1 pyramidal neurons was reported for *GluR-B^{-/-}* mice, which do not express GluR-B¹⁴, although the calcium permeability in those cells was comparable to that in *GluR-B^{neo/neo}* mice, which lack GluR-B(R). Thus, the residual GluR-B(Q) expression in the *GluR-B^{neo/neo}* mutant may facilitate AMPAR assembly¹⁵. Because *GluR-B^{-/-}* mice have relatively few deficits¹⁴, we surmise, in the absence of direct experimental comparison, that this phenotypic difference arises largely from differences in the macroscopic conductance of calcium-permeable AMPARs with and without GluR-B(Q) in principal neurons or from other property differences of AMPARs with and without GluR-B.

EFFECTS MEDIATED BY INCREASED CALCIUM INFLUX

We do not know the full range of synaptic and cellular effects caused by increased calcium influx through AMPARs in neurons that normally do not express calcium-permeable AMPARs. Although excessive calcium inflow through AMPARs can kill neurons², we found no evidence for ongoing cytotoxicity in the mutants; instead, the deleterious effects of calcium in our mutants seem to arise from altered network properties. The calcium-permeable AMPARs in pyramidal CA1 synapses of all mutants lead to a gain of function in the form of NMDAR-independent LTP, as also reported for GluR-B-

deficient mice¹⁴. Thus, calcium influx through AMPARs can partially substitute for influx through NMDARs in triggering long-lasting changes in synaptic efficacy, consistent with NMDAR-independent LTP in excitatory synapses where calcium-permeable AMPARs mediate EPSPs^{30,31}.

In *GluR-B^{neo/neo}* mutants, higher electrical stimulation was required to elicit fEPSPs, and the number of failures to induce LTP was increased compared to wild-type mice. These differences are likely to reflect deficits in dendritic arborization and reduced AMPAR numbers. Interestingly, increased stimulation intensity was also required in the *GluR-B^{-/-}* mutants¹⁴. If deficits in neuronal architecture were also verified for *GluR-B^{-/-}* mice, one would conclude that high calcium permeability of AMPARs can interfere with dendritic arborization during development. The calcium entering the postsynaptic cell via mutant AMPARs could rapidly desensitize NMDAR channels³⁶ colocalized in postsynaptic densities³⁷, and could, in turn, delay establishment or consolidation of synaptic connections and delay the development of dendritic arbors, as observed for CA3 neurons of *GluR-B^{neo/neo}* mice.

In summary, our findings show that manipulating GluR-B gene expression and the extent of Q/R site editing produces a wide range of phenotypes. In principle, if these factors were modulated in the brain, even modest alterations might affect synaptic function.

Methods

GENERATION OF GLUR-B(Q)-EXPRESSING MICE. *GluR-B^{+/neo}* mice were generated by injecting recombinant 129SV R1 ES cell clones¹³ into C57BL/6 blastocysts. Seven highly chimeric male animals did not have any offspring, possibly due to the presence of the viral *tk* gene in germ cells³⁸. Two other less-chimeric animals produced *GluR-B^{+/neo}* offspring. Intercrossing (F2) yielded *GluR-B^{+/+}*, *GluR-B^{+/neo}* and *GluR-B^{neo/neo}* mice in a ratio ~1:2:1. Mice were PCR genotyped with loxP flanking primer MH53 and *rsp36* (ref. 13). Amplicons were 494 bp from *GluR-B⁺*, 250 bp from *GluR-B^{ΔECS*}* and 3400 bp from *GluR-B^{neo}* allele. As an alternative, MH53 and *rsplox5* (5'-CACTGCTGACCTGAGCCAAG-3') were used: 211 bp for both the *GluR-B^{neo}* and the *GluR-B^{ΔECS*}* allele. Primers *Cre1* (5'-ACCAGTTCGTTCACTCATGG-3') and *Cre2* (5'-AGGCTAAGTGCCCTTCTCTACAC-3') demonstrated the presence of the Cre transgene by amplicons of 217 bp. Southern blots were done with probe 1 (400 bp *BglIII/KpnI* fragment) and probe 2 (800 bp *BglIII/HpaI* fragment).

RT-PCR, NORTHERN BLOTS AND *IN SITU* HYBRIDIZATION. RT-PCR was done with B52 and 3'lamlo¹³. Amplified fragments were subcloned and analyzed for Q/R site editing by differential hybridization¹². Northern blots were done on total brain RNA with membranes probed with GluR-B cDNA⁴³ and reprobated with a cyclophilin cDNA³⁹. *In situ* hybridization was done as described⁴⁰.

GLUR-B(N) TRANSGENE. A GluR-B(N) minigene was constructed from a 6-kb *EcoRI-KpnI* *BALB/c* genomic DNA fragment comprising over 5 kb of the upstream region, including the GluR-B promoter⁴¹, exon 1 and part of intron 1; plus a 1.1-kb *KpnI* fragment, itself the fusion of two PCR products connecting the murine intron1 sequence⁴² to rat GluR-B cDNA⁴³ (at the junction, in exon-2 codons for GluR-B residues FSTS, eight silent nucleotide substitutions were introduced with PCR primer Bex2, 5'-CTGAACCTCACTGGTACTGAACCTGAACCATCC-3'); plus a 2.2-kb *KpnI-EcoRV* fragment of GluR-B flip cDNA, mutated to contain an asparagine (N) codon for the Q/R site⁹; and finally a 0.6-kb *SmaI-SalI* fragment containing the transcriptional stop of the hGH gene⁴⁴. The transgene, assembled in pBlue-scriptSK(-), was isolated as a *NotI-SalI* fragment for pronucleus injection. Transgenic lines were analyzed by *in situ* hybridization (Bex2, GluR-B(N) specific, and Bx21, 5'-GCACCCTCCCATGCCTCACACAATCACCCTCTCT-3', detecting all GluR-B mRNA) and by hybridization of cloned GluR-B brain RT-PCR products with Bex2 and Bex2endo (5'-CTGAACCTCGAAGTGGAAAACCTGAACCATCC-3'), specific for the endogenous GluR-B. Line L238.2 showed highest expression.

WESTERN BLOTS. Membrane proteins of mouse brains were transferred to nitrocellulose membranes⁴⁵ and probed with T62-3B anti-GluR-B anti-

body⁴⁶ at 1 μg/ml and with peroxidase-linked anti-rabbit secondary antibody. The enhanced chemoluminescence method (Amersham Buchler GMBH&CoKG, Braunschweig, Germany) was used to detect GluR-B.

ELECTROPHYSIOLOGY. We used 300–400 μm hippocampal slices. Neuron identification and nucleated patch recordings were done as described¹³. Slices were superfused with extracellular solution (125 mM NaCl, 2.5 mM KCl, 25 mM NaHCO₃, 1.25 mM NaH₂PO₄, 2 mM CaCl₂ and 1 mM MgCl₂) that was bubbled with 95%O₂, 5%CO₂. AMPAR channel I–V relationships were measured in sodium-rich (135 mM NaCl, 5.4 mM KCl, 1.8 mM CaCl₂, 1 mM MgCl₂, 5 mM HEPES-NaOH, pH 7.2) and calcium-rich solutions (30 mM CaCl₂, 105 mM N-methyl-D-glucamine, 5 mM HEPES-HCl, pH 7.2) during 100-ms application of 1 mM glutamate via a theta-glass pipette. NMDAR currents were blocked with 100 μM D-2-amino-5-phosphonopentanoic acid (APV). The intracellular solution contained 140 mM CsCl, 10 mM EGTA, 2 mM MgCl₂, 2 mM adenosine triphosphate and 10 mM CsOH (pH 7.3). The P_{Ca}/P_{Na} ratios were determined from the reversal potentials obtained in sodium-rich (V_{revNa}) and calcium-rich solution (V_{revCa}) according to the equation: P_{Ca}/P_{Na} = 0.25a_{Na}/a_{Ca} {exp[(2V_{revCa} – V_{revNa})F/RT] + exp [(V_{revCa} – V_{revNa})F/RT]}, where a_{Na} and a_{Ca} are the activities of sodium and calcium in the extracellular solutions, respectively, and R, T, F have their conventional meaning²⁷. Activity coefficients were estimated by interpolation from tabulated values (0.75 for sodium and 0.55 for calcium). V_{revCa} and V_{revNa} were corrected for liquid junction potentials of 9.8 and 4.5 mV, respectively. The permeability ratios P_{Ca}/P_{Na} obtained from this equation were used to calculate P_f = 1/[1+(P_{Na}/P_{Ca}) (a_{Na}/a_{Ca}) (1 – exp(2V_mF/RT))/4] with 1.8 mM external calcium and membrane potential at –60 mV²⁷. The activity coefficient for 1.8 mM calcium was 0.57.

LTP EXPERIMENTS. Adult (three to four months old) and young (P11 to P17) mice were sacrificed with halothane. The brain was removed and cooled (0°C) in artificial cerebrospinal fluid (ACSF: 124 mM NaCl, 2 mM KCl, 1.25 mM KH₂PO₄, 2 mM MgSO₄, 2 mM CaCl₂, 26 mM NaHCO₃, 10 mM glucose, bubbled with 95% O₂, 5% CO₂, pH 7.4). A block containing the middle portion of the hippocampus was removed, and 400-μm transverse slices were cut with a vibraslicer in O₂, CO₂-bubbled ACSF. Slices were placed in an interface chamber (28–32°C) and exposed to humidified gas. To block NMDAR, 50 or 100 μM APV was added to the ACSF. Orthodromic synaptic stimulation (20–90 μs, < 100 μA, 0.2 Hz) in the CA1 region was delivered alternately through two tungsten electrodes to activate synapses at apical or basal dendrites. Extracellular responses were monitored by two glass electrodes, placed in the corresponding layers (Fig. 3a). After stable synaptic recordings had been obtained in both pathways for at least 15 min, one of the pathways was tetanized (100 Hz, 1 s). The tetanic stimulation strength was just above the threshold for generation of a population spike in response to a single stimulus. This procedure was used to adopt the same tetanization strength in different experiments. The pathway that was not activated during tetanization served as a control. Synaptic strength was assessed by measuring the slope of the fEPSP in the middle third of its rising phase. Six consecutive responses (1 min) were averaged and normalized to the mean value recorded 4–7 min before tetanic stimulation.

CYTOARCHITECTURE OF NEURONS. Whole-cell voltage recordings of CA1 and CA3 pyramidal neurons were done with patch pipettes containing 105 mM K-gluconate, 30 mM KCl, 10 mM HEPES, 4 mM ATP-Mg, 10 mM phosphocreatine and 0.3 mM GTP, pH 7.3, with 0.1–0.5% biocytin. After fixation in phosphate-buffered 4% paraformaldehyde, slices were incubated in avidin-conjugated horseradish peroxidase. Neurons were visualized using 3,3'-diaminobenzidine³⁴. Somata, apical and basal dendrites were reconstructed at a magnification of 400–1000× with the NEUROLUCIDA tracing system.

HISTOLOGY OF BARREL CORTEX. Cytochrome oxidase histochemistry was done on frozen 50-μm tangential sections of mouse brains⁴⁷, which were fixed for 1 h in 4% paraformaldehyde and cryoprotected for 24 h in 30% sucrose in 0.1% phosphate-buffered saline (PBS) containing 137 mM NaCl, 6.5 mM Na₂HPO₄, 2.7 mM KCl and 1.5 mM KH₂PO₄, pH 7.4. Cytochrome oxidase activity was visualized by incubation of mounted sections in 4% sucrose, 0.05% cytochrome C and 0.05% diaminobenzidine (Sigma-Aldrich Chemie GmbH, Deisenhofen, Germany).

Acknowledgements

We thank B. Sakmann and P. Andersen for discussions, R.J. Wenthold for antibodies, F. Schwenk for the deleter mouse, R. Pfeiffer, A. Herold, M. Lang for technical assistance and M. Belovska, M. Kosma, S. Kranz for dendritic tree analysis. K.K. was recipient of an EMBO long-term fellowship. H.-C.K. was supported by Boehringer Ingelheim. This work was funded, in part, by grants from HFSP, the Volkswagenstiftung, the German Chemical Society and an unrestricted grant from Bristol-Meyers Squibb.

RECEIVED 28 AUGUST; ACCEPTED 9 NOVEMBER 1998

- Katz, L. C. & Shatz, C. J. Synaptic activity and the construction of cortical circuits. *Science* **274**, 1133–1138 (1996).
- Bliss, T. V. & Collingridge, G. L. A synaptic model of memory: long-term potentiation in the hippocampus. *Nature* **361**, 31–39 (1993).
- Choi, D. W. Calcium: still center-stage in hypoxic-ischemic neuronal death. *Trends Neurosci.* **18**, 58–60 (1995).
- Rothstein, J. D. & Kuncl, R. W. Neuroprotective strategies in a model of chronic glutamate-mediated motor neuron toxicity. *J. Neurochem.* **65**, 643–651 (1995).
- Hollmann, M. & Heinemann, S. F. Cloned glutamate receptors. *Annu. Rev. Neurosci.* **17**, 31–108 (1994).
- Geiger, J. R. *et al.* Relative abundance of subunit mRNAs determines gating and Ca²⁺ permeability of AMPA receptors in principal neurons and interneurons in rat CNS. *Neuron* **15**, 193–204 (1995).
- Jonas, P. & Burnashev, N. Molecular mechanisms controlling calcium entry through AMPA-type glutamate receptor channels. *Neuron* **15**, 987–990 (1995).
- Hume, R. I., Dingledine, R. & Heinemann, S. F. Identification of a site in glutamate receptor subunits that controls calcium permeability. *Science* **253**, 1028–1031 (1991).
- Burnashev, N., Monyer, H., Seeburg, P. H. & Sakmann, B. Divalent cation permeability of AMPA receptor channels is dominated by the edited form of a single subunit. *Neuron* **8**, 189–198 (1992).
- Sommer, B., Köhler, M., Sprengel, R. & Seeburg, P. H. RNA editing in brain controls a determinant of ion flow in glutamate-gated channels. *Cell* **67**, 11–19 (1991).
- Seeburg, P.H., Higuchi, M. & Sprengel, R. RNA editing of brain glutamate receptor channels: mechanisms and physiology. *Brain Res. Rev.* **26**, 217–229 (1998).
- Higuchi, M. *et al.* RNA editing of AMPA receptor subunit GluR-B: a base-paired intron-exon structure determines position and efficiency. *Cell* **75**, 1361–1370 (1993).
- Brusa, R. *et al.* Early-onset epilepsy and postnatal lethality associated with an editing-deficient *GluR-B* allele in mice. *Science* **270**, 1677–1680 (1995).
- Jia, Z. *et al.* Enhanced LTP in mice deficient in the AMPA receptor GluR2. *Neuron* **17**, 945–956 (1996).
- Wenthold, R. J., Petralia, R. S., Blahos, J. II & Niedzielski, A. S. Evidence for multiple AMPA receptor complexes in hippocampal CA1/CA2 neurons. *J. Neurosci.* **16**, 1982–1989 (1996).
- Dong, H. *et al.* GRIP: a synaptic PDZ domain-containing protein that interacts with AMPA receptors. *Nature* **386**, 279–284 (1997).
- O'Brien, R. J., Lau, L.-F. & Haganir, R. L. Molecular mechanisms of glutamate receptor clustering at excitatory synapses. *Curr. Opin. Neurobiol.* **8**, 364–369 (1998).
- Lin, J. W. & Sheng, M. NSF and AMPA receptors get physical. *Neuron* **21**, 267–270 (1998).
- Swanson, G. T., Kamboj, S. K. & Cull-Candy, S. G. Single-channel properties of recombinant AMPA receptors depend on RNA editing, splice variation, and subunit composition. *J. Neurosci.* **17**, 58–69 (1997).
- Swanson, G. T., Feldmeyer, D., Kaneda, M. & Cull-Candy, S. G. Effect of RNA editing and subunit co-assembly on single-channel properties of recombinant kainate receptors. *J. Physiol. (Lond.)* **492**, 129–142 (1996).
- Mosbacher, J. *et al.* A molecular determinant for submillisecond desensitization in glutamate receptors. *Science* **266**, 1059–1062 (1994).
- Lomeli, H. *et al.* Control of kinetic properties of AMPA receptor channels by nuclear RNA editing. *Science* **266**, 1709–1713 (1994).
- Burnashev, N. Calcium permeability of glutamate-gated channels in the central nervous system. *Curr. Opin. Neurobiol.* **6**, 311–317 (1996).
- Washburn, M. S., Numberger, M., Zhang, S. & Dingledine, R. Differential dependence on GluR2 expression of three characteristic features of AMPA receptors. *J. Neurosci.* **17**, 9393–9406 (1997).
- Schwenk, F., Baron, U. & Rajewsky, K. A cre-transgenic mouse strain for the ubiquitous deletion of loxP-flanked gene segments including deletion in germ cells. *Nucl. Acids Res.* **23**, 5080–5081 (1995).
- Nagy, A. *et al.* Dissecting the role of N-myc in development using a single targeting vector to generate a series of alleles. *Curr. Biol.* **8**, 661–664 (1998).
- Burnashev, N., Zhou, Z., Neher, N. & Sakmann, B. Fractional calcium currents through recombinant GluR channels of the NMDA, AMPA and kainate receptor subtypes. *J. Physiol. (Lond.)* **485**, 403–418 (1995).
- Andersen, P., Sundberg, S. H., Sveen, O. & Wigström, H. Specific long-lasting potentiation of synaptic transmission in hippocampal slices. *Nature* **266**, 736–737 (1977).
- Kamal, A., Biessels, G. J., Gispen, W. H. & Urban, I. J. Increasing age reduces expression of long-term depression and dynamic range of transmission plasticity in CA1 field of the rat hippocampus. *Neuroscience* **83**, 707–715 (1998).
- Gu, J. G., Albuquerque, C., Lee, C. J. & MacDermott, A. B. Synaptic strengthening through activation of Ca²⁺ permeable AMPA receptors. *Nature* **381**, 793–796 (1996).
- Mahanty, N. K. & Sah, P. Calcium-permeable AMPA receptors mediate long-term potentiation in interneurons in the amygdala. *Nature* **394**, 683–687 (1998).
- Dunwiddie, T. V. & Lynch, G. The relationship between extracellular calcium concentrations and the induction of hippocampal long-term potentiation. *Brain Res.* **169**, 103–110 (1979).
- Wigström, H., Swann, J. W. & Andersen, P. Calcium dependency of synaptic long-lasting potentiation in the hippocampal slice. *Acta Physiol. Scand.* **105**, 126–128 (1979).
- Horikawa, K. & Armstrong, W. E. A versatile means of intracellular labeling: injection of biocytin and its detection with avidin conjugates. *J. Neurosci. Methods* **25**, 1–11 (1988).
- Kask, K. *et al.* The AMPA receptor subunit GluR-B in its Q/R site-unedited form is not essential for brain development and function. *Proc. Natl. Acad. Sci. USA* (in press).
- Kyrozis, A., Goldstein, P. A., Heath, M. J. S. & MacDermott, A. B. Calcium entry through a subpopulation of AMPA receptors desensitized neighboring NMDA receptors in rat dorsal horn. *J. Physiol. (Lond.)* **485**, 373–381 (1995).
- Kharazia, V. N., Phend, K. D., Rustioni, A. & Weinberg, R. J. EM colocalization of AMPA and NMDA receptor subunits at synapses in rat cerebral cortex. *Neurosci. Lett.* **210**, 37–40 (1996).
- Braun, R. E. *et al.* Infertility in male transgenic mice: disruption of sperm development by HSV-tk expression in postmeiotic germ cells. *Biol. Repr.* **43**, 684–693 (1990).
- Danielson, P. E. *et al.* p1B15: a cDNA clone of the rat mRNA encoding cyclophilin. *DNA* **7**, 261–267 (1988).
- Wisden, W. & Morris, B. J. in *In situ Hybridization Protocols for the Brain* (eds Wisden, W. & Morris, B. J.) 9–34 (Academic Press, San Diego, 1994).
- Myers, S. J. *et al.* Transcriptional regulation of the GluR2 gene: neural-specific expression, multiple promoters, and regulatory elements. *J. Neurosci.* **18**, 6723–6739 (1998).
- Köhler, M., Kornau, H.-C. & Seeburg, P. H. The organization of the gene for the functionally dominant alpha-amino-3-hydroxy-5-methylisoxazole-4-propionic acid receptor subunit GluR-B. *J. Biol. Chem.* **269**, 17367–17370 (1994).
- Sommer, B. *et al.* Flip and flop: a cell-specific functional switch in glutamate-operated channels of the CNS. *Science* **249**, 1580–1585 (1990).
- Chen, E. Y. *et al.* The human growth hormone locus: nucleotide sequence, biology, and evolution. *Genomics* **4**, 479–497 (1989).
- Sprengel, R. *et al.* Importance of the intracellular domain of NR2 subunits for NMDA receptor function in vivo. *Cell* **92**, 279–289 (1998).
- Petralia, R. S., Wang, Y. X., Mayat, E. & Wenthold, R. J. Glutamate receptor subunit 2-selective antibody shows a differential distribution of calcium-impermeable AMPA receptors among populations of neurons. *J. Comp. Neurol.* **385**, 456–476 (1997).
- Cases, O. *et al.* Lack of barrels in the somatosensory cortex of monoamine oxidase A-deficient mice: role of a serotonin excess during the critical period. *Neuron* **16**, 297–307 (1996).